American Mineralogist, Volume 107, pages 842–847, 2022

Chukochenite, $(Li_{0.5}Al_{0.5})Al_2O_4$, a new lithium oxyspinel mineral from the Xianghualing skarn, Hunan Province, China

Can Rao[1,*], Xiangping Gu[2], Rucheng Wang[3], Qunke Xia[1,†], Yuanfeng Cai[3,‡], Chuanwan Dong[1], Frédéric Hatert[4], and Yantao Hao[1]

[1]Key Laboratory of Geoscience Big Data and Deep Resource of Zhejiang Province, School of Earth Sciences, Zhejiang University, Hangzhou 310027, China
[2]School of Earth Sciences and Info-physics, Central South University, Changsha, 410083, China
[3]State Key Laboratory for Mineral Deposits Research, School of Earth Sciences and Engineering, Nanjing University, Nanjing, 210046, China
[4]Laboratoire de Minéralogie, B18, Université de Liège, B-4000 Liège, Belgium

Abstract

Chukochenite, $(Li_{0.5}Al_{0.5})Al_2O_4$, is a new mineral species from the Xianghualing skarn, Hunan Province, southern China. It occurs as subhedral to euhedral crystals up to 200 μm across in the green rock of Xianghualing skarn, closely associated with fluorite, phlogopite, chrysoberyl, margarite, chlorite, ferronigerite-2*N*1*S*, and zinconigerite-2*N*1*S*. The crystals are colorless and transparent with a vitreous luster. Chukochenite is brittle with irregular fracture, has a Mohs hardness of 8, and shows light red fluorescence under 253.7 nm UV radiation and light green fluorescence under 365 nm UV radiation. The calculated density is 3.771 g/cm^3. Chukochenite is optically biaxial (–) with $\alpha = 1.79(2)$, $\beta = 1.82(2)$, and $\gamma = 1.83(2)$ (589 nm). The calculated $2V$ is 60°, with the optical orientations *X*, *Y*, and *Z* parallel to the crystallographic *a*, *b*, and *c*, respectively. Electron microprobe analysis (Li by LA-ICP-MS) yielded in wt% Al_2O_3 80.70, Fe_2O_3 8.16, Li_2O 3.68, ZnO 3.25, MnO 2.49, MgO 1.70, Na_2O 0.11, CaO 0.08, TiO_2 0.02, K_2O 0.01, and Cr_2O_3 0.01 (total 100.24 wt%), giving an empirical formula $[(Li_{0.355}Al_{0.138}Na_{0.005}Ca_{0.002})_{\Sigma 0.5}(Al_{0.145}Fe^{+3}_{0.147}Mg_{0.061}Zn_{0.058}Mn_{0.051}Si_{0.001})_{\Sigma 0.463}]Al_2O_4$ on a basis of 4 O atoms per formula unit. Chukochenite is orthorhombic, *Imma*, $a = 5.659$ (1), $b = 16.898$ (1), $c = 7.994$ (1) Å, $V = 764.46$ (8) Å^3, and $Z = 12$. The nine strongest lines of powder XRD [*d* in Å (*I*) (*hkl*)] are: 2.405 (53) (231); 1.996 (29) (260); 1.535 (77) (303); 1.413 (100) (264); 1.260 (52) (2 12 0); 1.068 (36) (1 13 4); 1.039 (61) (503); 0.999 (59) (008); and 0.942 (35) (3 13 4). Chukochenite has a framework structure of spinel with low symmetry (orthorhombic *Imma*) due to the ordering of Li cations over octahedrally coordinated sites, which has not been previously reported for synthetic $(Li_{0.5}Al_{0.5})Al_2O_4$. This structure type is based on a framework of AlO_4 tetrahedra, AlO_6, and LiO_6 octahedra. AlO_6 edge-sharing octahedra form chains along the *a* axis. AlO_6 octahedra and LiO_6 octahedra in a 2:1 ratio share edges, forming octahedral chains along *b*. These octahedral chains are connected by AlO_4 tetrahedra and each corner of an AlO_4 tetrahedron shares with three AlO_6 octahedra or two AlO_6 + one LiO_6 octahedra. The discovery of chukochenite adds a new perspective on the cation ordering and the mechanism of luminescence and magnetism in $(Li_{0.5}Al_{0.5})Al_2O_4$.

Keywords: Chukochenite, new mineral, $(Li_{0.5}Al_{0.5})Al_2O_4$, crystal structure, optical property, XRD, EPMA, Raman spectroscopy; Lithium, beryllium, and boron: Quintessentially crustal

Introduction

The synthetic compound $(Li_{0.5}Al_{0.5})Al_2O_4$, when doped with trace metal ions such as Fe^{3+}, Eu^{3+}, Cr^{3+}, exhibits interesting magnetic and fluorescent properties, and thus the structures of two forms differing in cation ordering have been extensively studied for potential materials applications (e.g., Datta and Roy 1963; Pott and Mcnicol 1973; Singh and Rao 2008; Xie et al. 2011). Here, the corresponding natural phase, a new mineral chukochenite $(Li_{0.5}Al_{0.5})Al_2O_4$, but with a different structure of space group *Imma*, was found in the Xianghualing skarn, Linwu County, Hunan Province, China. Its petrographic features, chemical composition, and crystal structure were determined by optical microscopy, electron probe microanalysis, laser ablation-inductively coupled plasma-mass spectrometry (LA-ICP-MS), and X-ray diffraction. The new mineral is named after Chu Kochen (1890–1974), a famous scientist and educationist in China, who is known as the inaugurator of historical climatology, the leader of the "long march of academics," the founder of the Department of Geosciences at Zhejiang University, and, thus is recognized for making major contributions to science and education in China. The species and the name have been approved by the International Mineralogical Association, Commission on New Minerals, Nomenclature and Classification (CNMNC) (IMA 2018-132a) (Rao et al. 2020). The type sample of chukochenite is stored in the Geological Museum of China, Beijing, People's Republic of China, catalog number M13818. This paper reports the chemical

* E-mail: canrao@zju.edu.cn. Special collection papers can be found online at http://www.minsocam.org/MSA/AmMin/special-collections.html.
† Orcid 0000-0003-1256-7568
‡ Orcid 0000-0002-0182-3303

0003-004X/22/0005–842$05.00/DOI: https://doi.org/10.2138/am-2021-7932

composition and crystal structure of chukochenite, and compares this natural phase with its synthetic analogs of $(Li_{0.5}Al_{0.5})Al_2O_4$.

Occurrence and origin

Chukochenite was found in the green rock of the Xianghualing skarn, which is a tin-polymetallic (Sn-W-Be-Li) deposit in the Nanling Range, southern China. The Xianghualing skarn is located at the exocontact zone of the Laiziling granite, which intruded into the Middle-Upper Devonian carbonate rocks of the Qiziqiao Formation. The geological, mineralogical, and geochronological features of the Xianghualing skarn and the Laiziling granite have been extensively described in the literature (Chao 1964; Zhang and Wang 1986; Huang et al. 1988; Xiong et al. 2002; Yuan et al. 2007; Zhu et al. 2011; Yang et al. 2013a, 2013b; Huang et al. 2015; Rao et al. 2017; Xie et al. 2018; Wu et al. 2018). Like ribbon (Jahns 1944) or wrigglite rock (Kwak and Askins 1981), the Xianghualing skarn is composed of alternating light layers of fluorite ± other F-rich minerals and dark layers of Fe-rich minerals or Be-rich minerals. Large amounts of rare-metal minerals, such as Sn minerals (cassiterite, hulsite, and nigerite group minerals), W minerals (wolframite and scheelite), Be minerals (hsianghualite, liberite, chrysoberyl, hambergite, bertrandite, and taaffeite group minerals), and Li minerals (hsianghualite and liberite), occur in different layers, suggesting complex Sn, W, Be, and Li mineralizations of the Xianghualing skarn.

Chukochenite occurs as subhedral to euhedral crystals in the green rock of the Xianghualing skarn (Fig. 1). It is closely associated with fluorite, phlogopite, chrysoberyl, margarite, chlorite, ferronigerite-2*N*1*S*, and zinconigerite-2*N*1*S*, indicating that chukochenite is of hydrothermal origin and crystallized under F-rich conditions during the late stages of mineralization in the Xianghialing skarn. On the basis of fluid inclusions studies, Liu and Zeng (1998) suggested that Li mineralization at late stage of the Xianghualing skarn likely happened at 270–290 °C and 30–60 MPa. These values may represent the physical condition of chukochenite crystallization. Because of its relatively high concentrations of Li, Be, Sn, W, Rb, Nb, and Ta, the Laiziling granite is regarded as the main Li source of the Xianghualing orebodies, e.g., the average Li concentration in the Laiziling granite is 1615 ppm (Zhong 2014).

Physical and optical properties

Chukochenite crystals are up to 200 μm across (usually 50 to 100 μm) and are slightly heterogeneous under backscattered electron images (Fig. 1) due to variation in their ZnO contents. The crystals are colorless and transparent with vitreous luster, and they show light red and light green fluorescence under UV radiation of 253.7 and 365 nm, respectively. The Mohs hardness is about 8, close to that of chrysoberyl; the tenacity is brittle with irregular fracture. Based on the empirical formula and unit-cell parameters of chukochenite, its density is calculated to be 3.771 g/cm^3. Optically, chukochenite is biaxial (–), with α = 1.79(2), β = 1.82(2), and γ = 1.83(2) (589 nm). The calculated $2V$ is 60°, and optical orientation is $\alpha//a$, $\beta//b$, and $\gamma//c$. According to the calculated density and the measured indexes of refraction, the compatibility index $[1 - (K_P/K_C)]$ is 0.011, which belongs to the "excellent" category (Mandarino 1981).

Raman spectroscopy

A Raman spectrum of chukochenite was collected using a LabRAM HR evolution Laser Raman microprobe in the School of Earth Sciences, Zhejiang University. The spectrum was recorded from 100 to 4000 cm^{-1} with an accumulation time of 60 s using a 532 nm laser with a power of 50 mW. The spectrum (Fig. 2) was obtained from a chukochenite single crystal on a polished thin section. The Raman shifts at 827 and 754 cm^{-1} may be assigned to AlO_4 tetrahedra, while the Li-O and Al-O vibration modes in octahedra are probably at 692, 556, and 437 cm^{-1}. No Raman shifts are observed at 3400–3600 cm^{-1}, and thus there is no evidence for the presence of either H_2O or OH in the structure of chukochenite.

Chemical analysis

Chemical compositions of chukochenite were determined at the EPMA Lab (SHIMADZU EPMA-1720H; WDS; 15 kV; 20 nA; beam diameter = 1 μm) at Zhejiang University. Standards for the analysis were orthoclase (Na*K*α), $MnTiO_3$ (Ti*K*α),

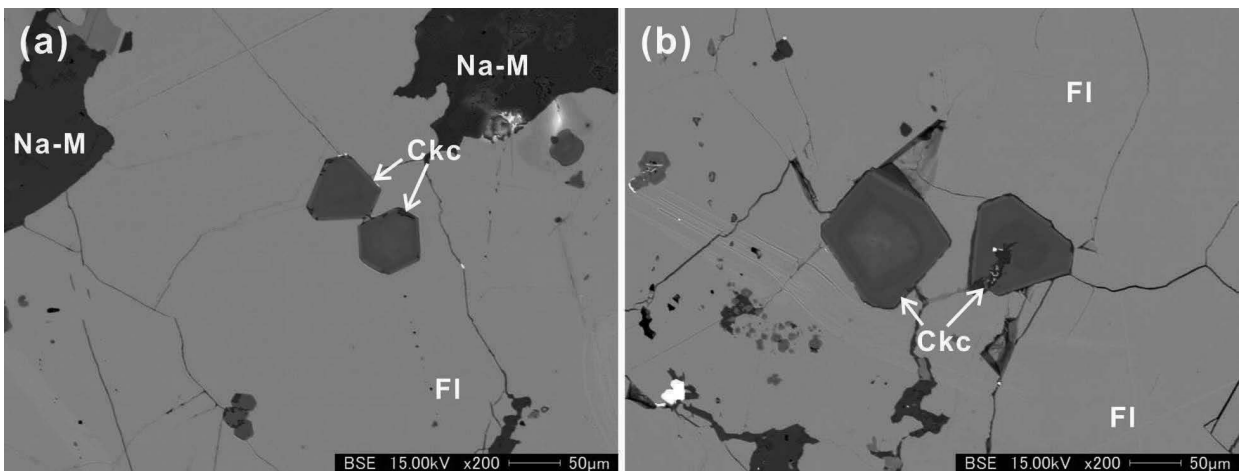

Figure 1. Backscattered electron images showing (**a**) occurrence and mineral associations of chukochenite and (**b**) euhedral chukochenite crystals among fluorite crystals. Abbreviations: Ckc = chukochenite; Fl = fluorite; Na-M = Na-matgarite.

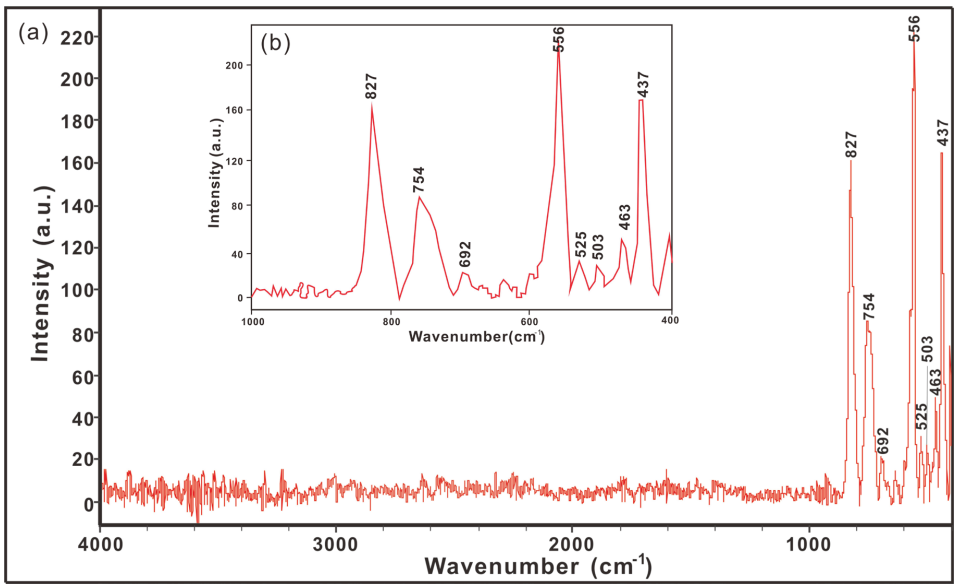

Figure 2. Raman spectrum of chukochenite. (Color online.)

almandine (Ca*K*α and Fe*K*α), obsidian (K*K*α), pyrope (Mg*K*α), willemite (Mn*K*α, Zn*K*α, and Si*K*α), topaz (Al*K*α), and chromite (Cr*K*α). The low analytical total from EPMA is due to the presence of Li_2O. Fluorine was not detected in the sample.

Li contents of chukochenite were measured by LA-ICP-MS at Zhejiang University. The laser was set at 6 Hz and 5 J/cm^2 energy per pulse, and the ablation times were typically 40 s. The signal intensities (counts per parts per million) for each element were calibrated against a NIST SRM 610 silicate glass standard (485 ppm Li), and the Fe content of chukochenite obtained by EPMA was used as an internal standard. The NITS SRM 612 with 42 ppm Li was also measured as an unknown to ensure the reliability of this method. The results from 6 spot analyses are 1.64–1.77 wt% Li, which is equivalent to 3.51–3.79 wt% Li_2O. Beryllium was not detected in chukochenite by LA-ICP-MS.

The chemical compositions of chukochenite are given in Table 1, which lead to an empirical formula $[(Li_{0.355}Al_{0.138}Na_{0.005}Ca_{0.002})_{\Sigma 0.5}(Al_{0.145}Fe^{3+}_{0.147}Mg_{0.061}Zn_{0.058}Mn_{0.051}Si_{0.001})_{\Sigma 0.463}]Al_2O_4$, based on 4 O atoms per formula unit (Bosi et al. 2019b). The idealized formula is $(Li_{0.5}Al_{0.5})Al_2O_4$, which corresponds to Al_2O_3 94.46 wt% and Li_2O 5.54 wt%.

Table 1. Chemical composition of chukochenite from the Xianghualing Skarn

	wt% (n = 31)	Range	St. dev.		apfu
Al_2O_3	80.70	75.68–86.03	2.47	Al	4.565
Fe_2O_3[a]	8.16	6.90–11.03	0.84	Fe^{3+}	0.295
Li_2O[b]	3.68	3.51–3.79	0.12	Li	0.711
ZnO	3.25	0.20–8.24	2.41	Zn	0.116
MnO	2.49	1.70–4.57	0.65	Mn	0.102
MgO	1.70	0.77–2.89	0.50	Mg	0.121
Na_2O	0.11	0–0.30	0.07	Na	0.010
CaO	0.08	0–0.52	0.13	Ca	0.004
SiO_2	0.04	0–0.15	0.03	Si	0.002
TiO_2	0.02	0–0.06	0.02	Ti	0.001
K_2O	0.01	0–0.01	0.01	K	0.000
Cr_2O_3	0.01	0–0.04	0.01	Cr	0.000
Total	100.24	99.06–100.97	0.46		

[a] Fe_2O_3 = calculated as trivalent.
[b] Li_2O = measured by LA-ICP-MS.

Powder X-ray diffraction

Powder X-ray diffraction (XRD) was performed with a Rigaku D/MAX RAPID II micro-diffractometer (Mo*K*α, λ = 0.71073 Å) at the State Key Laboratory for Mineral Deposits Research, School of Earth Sciences and Engineering, Nanjing University, China. The micro-diffractometer was operated with a curved imaging plate detector, under 40 kV and 100 mA, using a 0.3 mm diameter collimator. Data were collected from 8–179.0° 2θ with a step of 0.03° and a total exposure time of 2 h. We used the structural model obtained from single-crystal XRD (see below) to index the powder XRD pattern of chukochenite (Table 2). The nine strongest lines [*d* in Å (*I*) (*hkl*)] are: 2.405 (53) (231); 1.996 (29) (260); 1.535 (77) (303); 1.413 (100) (264); 1.260 (52) (2 12 0); 1.068 (36) (1 13 4); 1.039 (61) (503); 0.999 (59) (008); and 0.942 (35) (3 13 4). Unit-cell parameters calculated from powder XRD data are: a = 5.642(1) Å, b = 16.827(2) Å, c = 8.014(1) Å, and V = 760.80(2) Å^3.

Crystal structure determination

Single-crystal XRD measurements were carried out using a Rigaku Synergy diffractometer (Mo*K*α 50 kV, 1 mA) in the School of Earth Sciences and Info-physics, Central South University, China. One crystal fragment, measuring 40 × 35 × 20 μm, provided usable data to perform a structure refinement of chukochenite (CIF[1] available). These 550 frames with a spatial resolution of 0.5° were collected by the φ/ω scan technique, with a counting time of 20 s per frame, in the range 4.82° < 2θ < 67.42°. A total of 3670 reflections were extracted from these frames, corresponding to 758 unique reflections. The

TABLE 2. X-ray powder diffraction pattern (*d* in angstroms) of chukochenite and synthetic $(Li_{0.5}Al_{0.5})Al_2O_4$

Chukochenite				Synthetic $(Li_{0.5}Al_{0.5})Al_2O_4$[a]			Synthetic $(Li_{0.5}Al_{0.5})Al_2O_4$[b]		
I_{obs}	d_{obs}	$d_{cal.}$	*hkl*	*I*	*d*	*hkl*	*I*	*d*	*hkl*
12.7	8.501	8.450	020						
6.4	7.081	7.209	011	16.5	5.591	110			
7.6	4.593	4.601	031	5.8	4.565	111	**35.0**	**4.610**	**111**
5.3	3.107	3.112	051	15.2	3.536	210			
17.3	2.815	2.821	200	**38.6**	**2.795**	**220**	**25.0**	**2.821**	**220**
53.1	2.405	2.404	231	100	2.384	311	100.0	2.405	311
28.9	1.996	1.989	260	46.6	1.977	400	65.0	1.995	400
25.4	1.627	1.629	332	12.1	1.614	422	10	1.629	422
76.7	**1.535**	**1.538**	**303**	**33.1**	**1.521**	**511**	**40**	**1.536**	**511**
100.0	**1.413**	**1.412**	**264**	**63.2**	**1.398**	**440**	**75.0**	**1.410**	**440**
2.7	1.349	1.350	165				3	1.349	531
51.8	**1.260**	**1.256**	**2 12 0**				2	1.262	620
25.4	1.219	1.220	305				10.0	1.217	533
11.0	1.151	1.153	404				7.0	1.152	444
100.0[c]	1.116	1.116	0 15 1						
36.2	**1.068**	**1.068**	**1 13 4**						
60.7	**1.039**	**1.040**	**503**						
59.1	**0.999**	**0.999**	**008**						
100.0[c]	0.967	0.965	4 12 2						
34.8	**0.942**	**0.941**	**3 13 4**						

Note: Bold = strongest lines.
[a] Synthetic $(Li_{0.5}Al_{0.5})Al_2O_4$ with the space group *P*4132 (data from PDF No. 71-1736).
[b] Synthetic $(Li_{0.5}Al_{0.5})Al_2O_4$ with the space group $Fd\bar{3}m$ (data from PDF No. 31-0701).
[c] Peaks overlapping with fluorite peaks.

Rigaku CrystalClear software package was used for processing the structural data of chukochenite, including Lorentz and polarization corrections, and the application of an empirical absorption correction using the multi-scan method with ABSCOR (Higashi 2001). Unit-cell parameters refined from these reflections are $a = 5.659(1)$ Å, $b = 16.898(1)$ Å, $c = 7.994(1)$ Å, $V = 764.46(8)$ Å^3, and $Z = 12$. Careful inspection of the reflection data set indicated *Imma* as the most probable space group.

The crystal structure was determined and refined to $R = 0.0424$, based on 613 independent reflections with $I > 3\sigma(I)$ using the program package JANA2006 (Petříček et al. 2014). Atomic scattering factors for neutral atoms together with anomalous dispersion correction were taken from *International Tables for Crystallography* (Prince 2004). The site scattering factors were obtained by refining Al vs. Li on the Li1, Al1, Al3, and Al5 sites, and by refining Fe vs. Al on the Al2 and Al3 sites. The cationic distribution was established in agreement with the chemical data, site scattering factors and average bond distances (Table 3). Selected bond distances are given in Table 4, and bond valence analysis results are presented in Table 5.

The structure of chukochenite is based on a tetrahedral-octahedral framework (Fig. 3). Tetrahedra are mainly occupied by Al, with two sizes of AlO_4 tetrahedra (<Al2-O> = 1.793–1.828 Å and <Al4-O> = 1.917–1.936 Å), which are occupied by 0.87 Al + 0.13 Fe^{3+} and 0.32 Al +0.18 Mg + 0.17 Fe^{3+} + 0.17 Zn + 0.16 Mn, respectively (Table 3). Octahedra are occupied by Al and Li, corresponding to AlO_6 octahedra (<Al-O> = 1.883–1.955 Å) and LiO_6 octahedra (<Li-O> = 2.004–2.040 Å). The octahedral Al1, Al3, and Al6 sites are occupied by 0.95Al + 0.05 Li, 0.92 Al + 0.08 Li and 0.90 Al + 0.10 Li, respectively. The octahedral LiO_6 site is occupied by 0.70 Li + 0.30 Al. In the *b* direction, AlO_6 and LiO_6 octahedra in 2:1 ratio share edges, forming octahedral chains. In layers parallel to (010), AlO_6 octahedra form chains along the *a* axis via edge-sharing. AlO_4 tetrahedra occur between AlO_6-LiO_6 and AlO_6 octahedral chains; each corner of an AlO_4 tetrahedron shares with three AlO_6 octahedra or two AlO_6 + one LiO_6 octahedra. In fact, chukochenite is the first spinel mineral with the space group *Imma*, and belongs to a new lithium oxyspinel mineral (Bosi et al. 2019a). Chukochenite is isostructural with spinel supergroup minerals, but Li-bearing spinel has not been reported previously.

DISCUSSION

Chukochenite is a new mineral having the composition $(Li_{0.5}Al_{0.5})Al_2O_4$, identical to that of spinel compounds that have been studied extensively because of their fluorescence, phosphorescence, and magnetic properties when doped with trace elements. Synthetic $(Li_{0.5}Al_{0.5})Al_2O_4$ has two polymorphs: a low-temperature ordered phase with the space group $P4_132$ (e.g., Darul et al. 2007) and a high-temperature disordered phase with the space group $Fd\bar{3}m$ (e.g., Kutty and Nayak 1998). In contrast, chukochenite has the space group *Imma*, which has not been reported in synthetic $(Li_{0.5}Al_{0.5})Al_2O_4$. Powder XRD patterns of chukochenite and synthetic $(Li_{0.5}Al_{0.5})Al_2O_4$ compounds are largely similar (Table 2). However, there are several peaks with *d* values of 8.501, 7.081, 4.593, 3.107, and 2.815 Å in low diffraction angle region of chukochenite (Table 2) that cannot be explained by the structures of synthetic $(Li_{0.5}Al_{0.5})Al_2O_4$ compounds (e.g., Kutty and Nayak 1998; Xie et al. 2011). Therefore, chukochenite is not only the first natural spinel

TABLE 3. Cationic distribution in the structure of chukochenite

Site	Rss	Site-population (apfu)	CSS	ABL	CBL	VS	BVS
Li^{VI}	6.4	$Li_{0.70}Al_{0.30}$	6.0	2.016	2.093	1.60	1.58
$Al1^{VI}$	12.7	$Al_{0.95}Li_{0.05}$	12.5	1.920	1.946	2.90	2.83
$Al2^{IV}$	14.7	$Al_{0.87}Fe^{3+}_{0.13}$	14.7	1.808	1.783	3.00	2.72
$Al3^{VI}$	12.2	$Al_{0.92}Li_{0.08}$	12.2	1.924	1.953	2.84	2.77
$Al4^{IV}$	20.3	$Al_{0.32}Mg_{0.18}Fe^{3+}_{0.17}Zn_{0.17}Mn_{0.16}$	19.8	1.928	1.898	2.49	2.21
$Al5^{VI}$	12.5	$Al_{0.90}Li_{0.10}$	12.0	1.909	1.958	2.80	2.85

Notes: RSS = refined site scattering factor (e^-); CSS = calculated site scattering factor (e^-); ABL = average observed bond-lengths (Å); CBL = calculated bond-lengths (Å); VS = theoretical bond-valence sums (v.u.); BVS = calculated bond-valence sums (v.u.). Ideal bond-distances were calculated using the ionic radii of Shannon (1976), and the bond-valence parameters were taken from Brown and Altermatt (1985).

TABLE 4. Selected bond distances (angstroms) in chukochenite

Li-O1(×2)	2.040(3)	Al3-O2(×2)	1.883(3)	Al4-O2(×2)	1.936(3)
Li-O3(×4)	2.004(2)	Al3-O5(×4)	1.945(2)	Al4-O4(×2)	1.917(3)
<Li-O>	2.016	<Al-O>	1.924	<Al-O>	1.927
Al1-O1(×2)	1.905(2)	Al2-O1	1.793(3)	Al5-O2(×2)	1.920(2)
Al1-O3(×2)	1.931(2)	Al2-O3(×2)	1.805(2)	Al5-O3(×2)	1.880(2)
Al1-O4(×2)	1.925(2)	Al2-O5	1.828(3)	Al5-O4	1.900(3)
<Al-O>	1.920	<Al-O>	1.808	Al5-O5	1.955(3)
				<Al-O>	1.909

TABLE 5. Bond valence sums for chukochenite

	Li	Al1	Al2	Al3	Al4	Al5	Σ
O1	0.258 (×2↓)	0.529(×2→) (×2↓)	0.672				1.99
O2				0.542 (×2↓)	0.519 (×2↓)	0.44(×2→) (×2↓)	1.94
O3	0.278 (×4↓)	0.494 (×2↓)	0.656 (×2↓)			0.487 (×2↓)	1.92
O4		0.498(×2→) (×2↓)			0.519 (×2↓)	0.468	1.98
O5			0.629	0.461(×2→) (×4↓)		0.408	1.96
Σ	1.63	3.04	2.61	2.93	2.08	2.73	

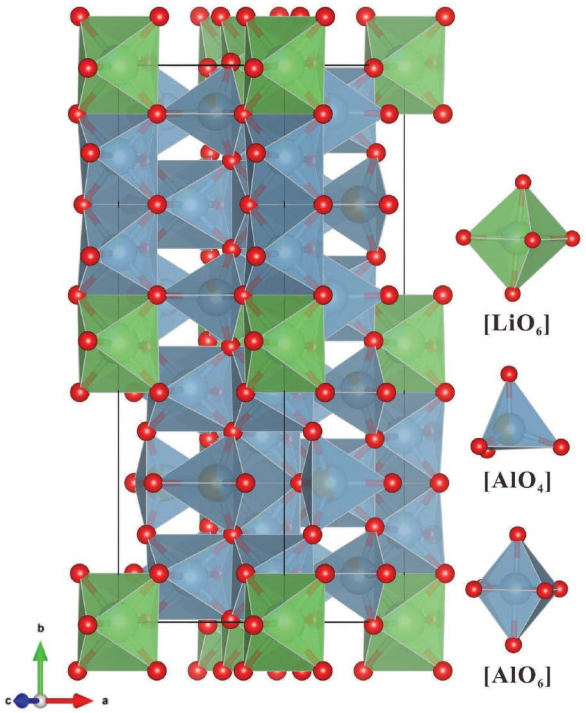

FIGURE 3. Structural model of chukochenite. (Color online.)

supergroup mineral containing Li but also the first to have the *Imma* symmetry. Nonetheless, the structures of chukochenite and synthetic $(Li_{0.5}Al_{0.5})Al_2O_4$ show a framework of tetrahedra and octahedra that is isostructural with that of the spinel supergroup (Peterson et al. 1991; Bosi et al. 2019a). Of greatest interest are the sites occupied by Li. In the chukochenite structure (Fig. 3), Li occupies octahedrally coordinated sites, and LiO_6 and AlO_6 octahedra form edge-sharing octahedral chains. The Li site is occupied by 0.70 Li, while the three Al octahedrally coordinated sites are occupied by 0.05 Li, 0.08 Li, and 0.10 Li, respectively. Each LiO_6 octahedron shares edges with six AlO_6 octahedra and shares corners with six AlO_6 tetrahedra. Li is absent in the tetrahedrally coordinated sites in the synthetic $(Li_{0.5}Al_{0.5})Al_2O_4$ structures, and the octahedrally coordinated sites are occupied by Li and Al with 1:3 ratio (Famery et al. 1979). The different Li atomic arrangements between two synthetic $(Li_{0.5}Al_{0.5})Al_2O_4$ phases result in the ordered and disordered states in the octahedral sites (Darul et al. 2007; Xie et al. 2011). The primitive cubic ordered $(Li_{0.5}Al_{0.5})Al_2O_4$ phase has a 1:3 Li:Al ordering in the octahedrally coordinated sites; each Li is surrounded by six Al atoms and each Al is surrounded by two Li and four Al atoms. In contrast, the spinel form of $(Li_{0.5}Al_{0.5})Al_2O_4$ has a disordered structure of Li and Al over octahedrally coordinated sites. Therefore, the different $(Li_{0.5}Al_{0.5})Al_2O_4$ structures are determined by the occupancy and distribution of Li in octahedrally coordinated sites.

In fact, chukochenite is generally isostructural with the two synthetic $(Li_{0.5}Al_{0.5})Al_2O_4$ phases. Its lower symmetry (orthorhombic *Imma*) is in large part due to Li^+ ordering, but the framework structure of spinel remains. The unit cell of chukochenite can be derived from that of synthetic spinel $(Li_{0.5}Al_{0.5})Al_2O_4$. Relative to the unit cell of synthetic $(Li_{0.5}Al_{0.5})Al_2O_4$, the unit cell of chukochenite is rotated 45° around *c* axis (Fig. 4). Therefore, the unit cell of chukochenite can be obtained by $a = c$ (7.994 Å) × cos 45° = 5.683 Å, $b = 3 \times a = 16.958$ Å, and $V = 1.5 \times V'$ (7.9943 Å^3) = 766.27 Å^3.

IMPLICATIONS

$(Li_{0.5}Al_{0.5})Al_2O_4$ adopts a series of polymorphs: disordered spinel $(Li_{0.5}Al_{0.5})Al_2O_4$ ($Fd\bar{3}m$) → ordered $(Li_{0.5}Al_{0.5})Al_2O_4$ ($P4_132$) → chukochenite (*Imma*). With increasing Li ordering, the symmetry decreases, but there is no change in the spinel framework topology. Therefore, the discovery of chukochenite draws attention to cation ordering during transitions between different $(Li_{0.5}Al_{0.5})Al_2O_4$ polymorphs. While synthetic $(Li_{0.5}Al_{0.5})Al_2O_4$ transforms from the disordered $Fd\bar{3}m$ phase to the ordered $P4_132$ phase, the ordering of $(Li_{0.5}Al_{0.5})Al_2O_4$ phases in nature

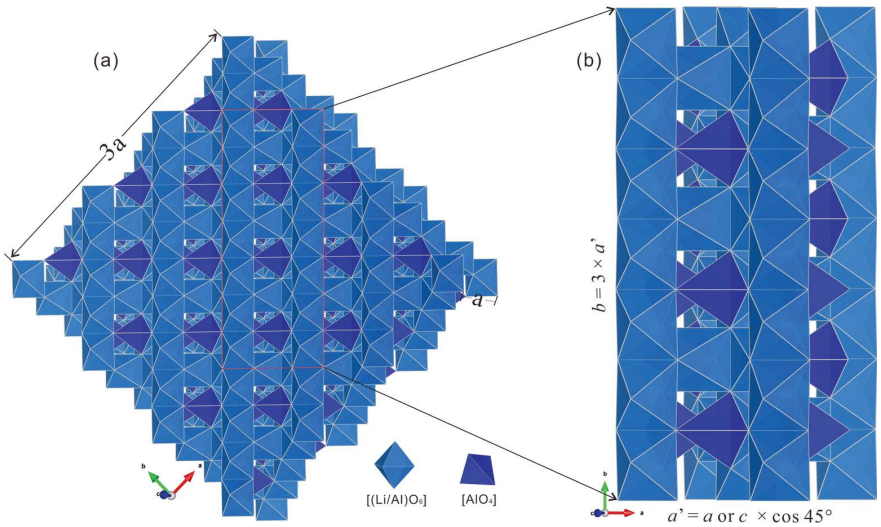

FIGURE 4. Geometrical relationship of the two unit-cells between (**a**) synthetic $(Li_{0.5}Al_{0.5})Al_2O_4$ and (**b**) chukochenite. (Color online.)

likely follows a different ordering path, ending with chukochenite. Under ambient, dry conditions, the transition between two synthetic $(Li_{0.5}Al_{0.5})Al_2O_4$ phases was indicated to happen around 1295 ± 5 °C (e.g., Braun 1952; Datta and Roy 1963; Kutty and Nayak 1998), but chukochenite (highly ordered, *Imma*) from the Xianghualing skarn likely crystallized from aqueous fluids at 270–290 °C and 30–60 MPa (Liu and Zeng 1998). The intimate intergrowths of chukochenite with fluorite (Fig. 1) suggest that the crystallization occurred under F-rich conditions during the late stages of hydrothermal metasomatism in the Xianghualing skarn. This feature may indicate that high fluorine activity could promote Li^+ ordering in the spinel structure. However, more than one path may happen between the completely disordered and the fully ordered $(Li_{0.5}Al_{0.5})Al_2O_4$ phases during different geological processes. Hence, future work on multiple ordering paths in $(Li_{0.5}Al_{0.5})Al_2O_4$ is needed.

Acknowledgments and Funding

We thank Ulf Hålenius, Edward S. Grew, Ferdinando Bosi, an anonymous reviewer, and Editor Hongwu Xu for their very helpful comments on the manuscript, which greatly improved its quality. Financial support for the research was provided by NSF of China (Grant No. 41772031).

References cited

Bosi, F., Biagioni, C., and Pasero, M. (2019a) Nomenclature and classification of the spinel supergroup. European Journal of Mineralogy, 31, 183–192.

Bosi, F., Biagioni, C., and Oberti, R. (2019b) On the chemical identification and classification of minerals. Minerals, 9, 591.

Braun, P.B. (1952) A superstructure in spinels. Nature, 170, 1123–1131.

Brown, I.D., and Altermatt, D. (1985) Bond-valence parameters obtained from a systematic analysis of the inorganic crystal-structure database. Acta Crystallographica Section B Structural Science, 41, 244–247.

Chao, C.L. (1964) Liberite Li_3BeSiO_4, a new lithium-beryllium silicate mineral from the Nanling Ranges, South China. Acta Mineralogica Sinica, 44, 334–342. (in Chinese with English abstract). American Mineralogist, 50, 519 (abstract).

Darul, J., Nowicki, W., Piszora, P., and Wolska, E. (2007) Synchrotron X-ray powder diffraction studies of solubility limits in the $LiFe_5O_8$-$LiAl_5O_8$ spinel solid solutions. Zeitschrift für Kristallographie Supplements, 2007, 471–476.

Datta, R.K., and Roy, R. (1963) Phase transitions in $LiAl_5O_8$. Journal of the American Ceramic Society, 46, 388–390.

Famery, R., Queyroux, F., Gilles, J.C., and Herpin, P. (1979) Etude structurale de la forme ordonnée de $LiAl_5O_8$. Journal of Solid State Chemistry, 30, 257–263.

Higashi, T. (2001) ABSCOR, Tokyo. Rigaku Corporation.

Huang, Y.H., Du, S.H., and Zhou, X.Z. (1988) Hsianghualing rocks, deposits and minerals, p. 115–116 Scientific Technique Press. (in Chinese).

Huang, F.F., Wang, R.C., Xie, L., Zhu, J.C., Erdmann, S., Che, X.D., and Zhang, R.Q. (2015) Diffffferentiated rare-element mineralization in an ongonite–topazite composite dike at the Xianghualing tin district, Southern China: an electron-microprobe study on the evolution from niobium-tantalum-oxides to cassiterite. Ore Geology Reviews, 65, 761–778.

Jahns, R.H. (1944) Ribbon rock", an unusual beryllium-bearing tactite. Economic Geology, 39, 173–205.

Kutty, T.R.N., and Nayak, M. (1998) Cationic distribution and its influence on the luminescent properties of Fe^{3+}-doped $LiAl_5O_8$ prepared by wet chemical methods. Journal of Alloys and Compounds, 269, 75–87.

Kwak, T.A.P., and Askins, P.W. (1981) The nomenclature of carbonate replacement deposits, with emphasis on Sn-F-Be-Zn "wrigglite" skarns. Journal of the Geological Society of Australia, 28, 123–136.

Liu, J.Q., and Zeng, Y.S. (1998) Preliminary study on fluid inclusions in hsianghualite. Huanan Dizhi Yu Kuangchan, 56–63.

Mandarino, J.A. (1981) The Gladstone-Dale relationship. IV. The compatibility concept and its application. Canadian Mineralogist, 19, 441–450.

Peterson, R.C., Lager, G.A., and Hitterman, R.L. (1991) A time-of-flight neutron powder diffraction study of $MgAl_2O_4$ at temperatures up to 1273 K. American Mineralogist, 76, 1455–1458.

Petříček, V., Dusek, M., and Palatinus, L. (2014) Crystallographic computing system. Zeitschrift für Kristallographie—Crystalline Materials, 229, 345–352.

Pott, G.T., and Mcnicol, B.D. (1973) Luminescence of Cr^{3+} ions in ordered and disordered $LiAl_5O_8$. Journal of Solid State Chemistry, 7, 132–137.

Prince, E. (Ed.) (2004) International Tables for Crystallography, Volume C: Mathematical, Physical and 354 Chemical Tables, 3rd ed. Kluwer Academic Publishers.

Rao, C., Hatert, F., Dal Bo, F., Wang, R.C., Gu, X.P., and Baijot, M. (2017) Mengxianminite $(Ca_2Sn_2Mg_3Al_8[(BO_3)(BeO_4)O_6]_2)$ a new borate mineral from Xianghualing skarn, Hunan Province, China, with a highly unusual chemical combination (B + Be + Sn.). American Mineralogist, 102, 2136–2141.

Rao, C., Gu, X.P., Wang, R.C., Xia, Q.K., Cai, Y.F., Dong, C.W., Hatert, F., and Hao, Y.T. (2020) Chukochenite, IMA 2018-132a. CNMNC Newsletter No. 54. European Journal of Mineralogy, 32, 275–283.

Shannon, R.D. (1976) Revised crystal ionic radii and systematic study of interatomic distances in halides and chalcogenides. Acta Crystallographica Section A, 32, 751–767.

Singh, V., and Rao, T.K.G. (2008) Studies of defects in combustion synthesized europium-doped $LiAl_5O_8$ red phosphor. Journal of Solid State Chemistry, 181, 1387–1392.

Wu, J.H., Li, H., Algeo, T.J., Jiang, W.C., and Zhou, Z.K. (2018) Genesis of the Xianghualing Sn-Pb-Zn deposit, South China: A multi-method zircon study. Ore Geology Reviews, 102, 220–239.

Xie, L., Wang, Z.J., Wang, R.C., Zhu, J.C., Che, X.D., Gao, J.F., and Zhao, X. (2018) Mineralogical constraints on the genesis of W–Nb–Ta mineralization in the Laiziling granite (Xianghualing district, south China). Ore Geology Reviews, 95, 695–712.

Xie, L.M., Yang, D.M., Wei, L., Hu, Y.M., and Ji, H.X. (2011) Synthesis and luminescence properties of plate-like europium ion doped $LiAl_5O_8$. Journal of Synthetic Crystals, 40, 684–688.

Xiong, X.L., Rao, B., Chen, F.R., Zhu, J.C., and Zhao, Z.H. (2002) Crystallization and melting experiments of a fluorine-rich leucogranite from the Xianghualing pluton, South China, at 150 MPa and H_2O-saturated conditions. Journal of Asian Earth Sciences, 21, 175–188.

Yang, Z.M., Ding, K., Fourestier, J.D., Mao, Q., and Li, H. (2013a) Fe-rich Li-bearing magnesio nigerite-6*N*6*S* from Xianghualing tin-polymetallic ore field, Hunan Province. Mineralogy and Petrology, 107, 163–169.

Yang, Z.M., Fourestier, J.D., Ding, K., and Li, H. (2013b) Li-bearing ferronigerite-2*N*1*S* from Xianghualing tin-polymetallic ore field, Hunan Province, China. Canadian Mineralogist, 51, 913–919.

Yuan, S., Peng, J., Shen, N., Hu, R., and Dai, T. (2007) ^{40}Ar-^{39}Ar isotopic dating of the Xianghualing Sn-polymetallic ore field in Southern Hunan, China and its geological implications. Acta Geologica Sinica, 81, 278–286. in Chinese, English Abstract).

Zhang, D.Q., and Wang, L.H. (1986) Metasomatism and zonation of the Xianghualing Tin-polymetallic deposit. Bulletin of the Institute of Mineral Deposits Chinese Academy of Geological Sciences, 2, 144–154.

Zhong, J.L. (2014) Major types and prospecting direction of nonferrous and rare polymetallic ore deposit in Xianghualing area, South China. Geology and Mineral Resource of South China, 30, 99–108.

Zhu, J.C., Wang, R.C., Lu, J.J., Zhang, H., Zhang, W.L., Xie, L., and Zhang, R.Q. (2011) Fractionation, evolution, petrogenesis and mineralization of Laiziling granite pluton, Southern Hunan Province. Geological Journal of China Universities, 17, 381–392.

Manuscript received December 14, 2020
Manuscript accepted May 4, 2021
Manuscript handled by Fabrizio Nestola

Endnote:

[1]Deposit item AM-22-57932, Online Materials. Deposit items are free to all readers and found on the MSA website, via the specific issue's Table of Contents (go to http://www.minsocam.org/MSA/AmMin/TOC/2022/May2022_data/May2022_data.html). The CIF has been peer reviewed by our Technical Editors.